NASA
Technical
Paper
2003

April 1982

Harmonic Well Matter Densities and Pauli Correlation Effects in Heavy-Ion Collisions

Lawrence W. Townsend

NASA

NASA Technical Paper 2003

1982

Harmonic Well Matter Densities and Pauli Correlation Effects in Heavy-Ion Collisions

Lawrence W. Townsend
Langley Research Center
Hampton, Virginia

National Aeronautics and Space Administration

Scientific and Technical Information Branch

INTRODUCTION

Accurate theoretical descriptions (refs. 1 to 3) of high-energy heavy-ion scattering phenomena require knowledge of nuclear single-particle density distributions (i.e., matter densities). Experimentally determined nuclear density distributions, however, are limited to charge and magnetization densities, obtained from electron scattering experiments. Extensive tables of nuclear charge distribution parameters exist (refs. 4 and 5). In practice, the charge densities are usually directly substituted for the matter densities where required in the analyses. The resultant theoretical cross sections, however, are typically overestimates (refs. 3, 6, and 7). As discussed in reference 3, these overestimates are a result of the increased surface diffuseness of the nuclear charge distributions over that of the matter distributions because of the finite spatial extent of the proton charge. In references 2 and 3, a method for extracting matter density distributions from Woods-Saxon charge densities was presented in conjunction with a generalized optical-model reaction theory for heavy-ion scattering. Although Woods-Saxon distributions are adequate for many nuclei, a better representation for the charge distribution of light and medium-weight nuclei (three to eight protons) is the harmonic well distribution (refs. 4, 5, and 8) based upon the nuclear shell model (ref. 9). In this paper, the general method of references 2 and 3 is applied to obtain matter densities from harmonic well charge densities. Unlike the Woods-Saxon distribution (used in refs. 2 and 3), which requires some analytic approximations to obtain the resultant matter density expression, the harmonic well distribution is exactly solvable.

As developed in references 2, 3, and 10, the heavy-ion reaction theory ignores the Pauli exclusion principle (Pauli correlation effects) by using simple products of wave functions rather than properly antisymmetric ones for calculating nuclear matrix elements. Although unimportant in estimating total and absorption cross sections for high-energy heavy-ion collisions (ref. 2), these Pauli correlation effects become significant when determining projectile-nucleus abrasion cross sections for small residual fragment masses (i.e., when there is large overlap between projectile and target nuclear volumes). In this paper, a method for incorporating these effects into the heavy-ion reaction model is presented. Finally, cross sections for selected nuclei are predicted with the improved optical potential model.

HARMONIC WELL MATTER DENSITIES

For relatively light nuclei with incomplete 1p shells, the harmonic well charge density (refs. 4, 5, and 8) is given by

$$\rho(r) = \rho_o\left[1 + \alpha\left(\frac{r}{a}\right)^2\right] \exp\frac{-r^2}{a^2} \tag{1}$$

where ρ_o is a normalization constant, r is the radial coordinate, the parameter α is some simple function of Z, the nucleus proton number,

$$\alpha = f(Z) \tag{2}$$

and a is the "oscillator parameter" given by

$$a = (m\omega_{osc})^{-1/2} \tag{3}$$

where m is the nucleon mass, 938 MeV/c^2. In equation (3), ω_{osc} is the equidistant-energy interval between successive oscillator levels (ref. 8). Rather than determining α from some specific functional dependence on Z, it is sometimes treated as a free parameter. Equation (1) is then referred to as a "modified" harmonic well charge density. Specific values for α and a, for the nuclei of interest, are tabulated in references 4 and 5. Values of the normalization constant ρ_o are obtained by requiring that

$$4\pi \int_0^\infty r^2 \rho(r)\, dr \equiv 1 \tag{4}$$

The matter density is related to the harmonic well charge density through the expression

$$\rho_c(\vec{r}) \approx \int \rho_p(\vec{r}')\, \rho_m(\vec{r}+\vec{r}')\, d^3\vec{r}' \tag{5}$$

where $\rho_c(\vec{r})$ is the nucleus charge density, $\rho_p(\vec{r})$ is the proton charge density, and $\rho_m(\vec{r})$ is the desired nuclear matter density. Equation (5) implies the assumption that the neutron and proton number densities within the nucleus are identical. This is reasonable since they differ only because of Coulomb repulsion between the protons which is a small effect in lighter nuclei. Taking the Fourier transform of equation (5) and using the convolution theorem yield a simple product of form factors:

$$F_c(q) = F_p(q)\, F_m(q) \tag{6}$$

where

$$F(q) = \frac{4\pi}{q} \int_0^\infty r(\sin qr)\, \rho(r)\, dr \tag{7}$$

and q is the magnitude of the momentum transfer.

From equations (1) and (7), the nuclear charge form factor is

$$F_c(q) = \rho_o \pi^{3/2} a^3 \left(1 + \frac{3\alpha}{2} - \frac{\alpha q^2 a^2}{4}\right) \exp \frac{-q^2 a^2}{4} \tag{8}$$

The usual form (refs. 4 and 8) for the proton charge density is a Gaussian function:

$$\rho_p(\vec{r}) = \left(\frac{3}{2\pi r_p^2}\right)^{3/2} \exp\frac{-3r^2}{2r_p^2} \tag{9}$$

where $r_p \approx 0.87$ fm (ref. 11) is the proton root-mean-square charge radius. From equation (7), the proton charge form factor is

$$F_p(q) = \exp\frac{-q^2 r_p^2}{6} \tag{10}$$

Hence, equations (6), (8), and (10) yield a matter density form factor of

$$F_m(q) = \rho_o \pi^{3/2} a^3 \left(1 + \frac{3\alpha}{2} - \frac{\alpha q^2 a^2}{4}\right) \exp(-q^2 s^2) \tag{11}$$

where

$$s^2 = \frac{a^2}{4} - \frac{r_p^2}{6} \tag{12}$$

The matter density is obtained by utilizing the inverse Fourier transform of the matter density form factor:

$$\rho_m(r) = \frac{1}{2\pi^2 r} \int_0^\infty q(\sin qr)\, F_m(q)\, dq \tag{13}$$

Substituting equation (11) into equation (13) yields

$$\rho_m(r) = \frac{\rho_o a^3}{8s^3}\left(1 + \frac{3\alpha}{2} - \frac{3\alpha a^2}{8s^2} + \frac{\alpha a^2 r^2}{16 s^4}\right) \exp\frac{-r^2}{4s^2} \tag{14}$$

Table I lists the values for α and a, taken from reference 5, which are substituted into equations (1) and (14) to determine the charge and matter density distributions. These results are plotted in figures 1 through 6 for six nuclei.

PAULI CORRELATION EFFECTS

Since nucleons have half-integer intrinsic spins (i.e., they are fermions), they must obey the Pauli exclusion principle. This principle requires the overall system wave function to be antisymmetric under the exchange of any two nucleons in the system. For a system composed of only two nucleons, the properly antisymmetric wave function is

$$\psi(1,2) = 2^{-1/2}[\phi_\alpha(1)\ \phi_\beta(2) - \phi_\alpha(2)\ \phi_\beta(1)] \tag{15}$$

where ϕ_α and ϕ_β are the wave functions for the nucleons. The product,

$$\phi_\alpha(1)\ \phi_\beta(2)$$

is usually called the direct term. Subtracted from the direct term is a product representing the exchange of coordinates of the two nucleons. This product,

$$\phi_\alpha(2)\ \phi_\beta(1)$$

is sometimes called the exchange term.

Previous versions of the optical-model reaction and fragmentation theories (refs. 2, 3, and 10) neglected antisymmetry and used only product wave functions (the direct term in eq. (15)). For determinations of heavy-ion total and absorption cross sections, neglect of antisymmetry is not an extreme assumption since the largest contributions to these cross sections come from peripheral collisions where there is little or no overlap between colliding nuclei (see "Results"). Pauli correlation effects, however, are significant when predicting projectile abrasion cross sections, particularly for small residual mass fragments (when there is significant overlap between the volumes of the colliding nuclei).

In references 2, 3, and 7, the optical potential operator is

$$V_{opt} = \sum_{\alpha j} t_{\alpha j} \tag{16}$$

where $t_{\alpha j}$ is the two-body transition amplitude between the α-constituent of the target and the j-constituent of the projectile. The expression in equation (16) is general in that it was derived independently of any specific assumptions regarding nuclear wave functions. In references 2 and 3, it was shown that for a simple product of wave functions, equation (16) yields for the optical potential

$$W(\vec{x}) = A_P A_T \int d^3\vec{\xi}_T\ \rho_T(\vec{\xi}_T) \int d^3\vec{y}\ \rho_P(\vec{x}+\vec{y}+\vec{\xi}_T)\ \tilde{t}(e,\vec{y}) \tag{17}$$

where

A_P, A_T	nuclear mass numbers of the projectile and target
e	two-nucleon kinetic energy in their center of mass frame, GeV
$\vec{x}$	relative position vector of the projectile, fm
$\vec{y}$	two-nucleon relative position vector, fm
$\vec{\xi}$	collection of constituent relative coordinates for target, fm

and the average two-nucleon transition amplitude is

$$\tilde{t}(e,\vec{y}) = \frac{1}{A_P A_T} \sum_{\alpha j} t_{\alpha j} \tag{18}$$

Equation (17) is a valid representation for the direct term, but does not include any Pauli correlation effects. In the following sections, equation (17) is generalized to include the exchange (correlation) effects.

Second Quantization Notation

In terms of second quantization notation (ref. 12), a two-body operator can be expressed as

$$G = \frac{1}{2} \sum_{ik} \sum_{\ell m} (ik|g|\ell m) b_k^\dagger b_i^\dagger b_\ell b_m \tag{19}$$

where b_γ is an annihilation operator and $b_\gamma^\dagger$ a creation operator for a nucleon in the single-particle state γ ($\gamma = i,k,\ell,m$). The matrix element in equation (19) is given by

$$(ik|g|\ell m) = \int d^3\vec{x}_1 \int d^3\vec{x}_2 \; \phi_i^\dagger(\vec{x}_1) \; \phi_k^\dagger(\vec{x}_2) \; g(\vec{x}_1,\vec{x}_2) \; \phi_\ell(\vec{x}_1) \; \phi_m(\vec{x}_2) \tag{20}$$

In this notation, a two-particle state is written as

$$|\ell m\rangle = b_\ell^\dagger b_m^\dagger |0\rangle \tag{21}$$

where $|0\rangle$ is the vacuum state. Thus, in terms of the two-particle state, the two-body operator is

$$\langle ik|G|\ell m\rangle = \frac{1}{2} \sum_{i'k'} \sum_{\ell'm'} (i'k'|g|\ell'm') \langle 0|b_k b_i b_{k'}^\dagger, b_{i'}^\dagger, b_{\ell'}, b_{m'}, b_{\ell'}^\dagger b_{m'}^\dagger|0\rangle \tag{22}$$

The operator commutator relations are

$$\left.\begin{aligned} b_i b_k + b_k b_i &= 0 \\ b_i^\dagger b_k^\dagger + b_k^\dagger b_i^\dagger &= 0 \\ b_i b_k^\dagger + b_k^\dagger b_i &= \delta_{ik} \end{aligned}\right\} \tag{23}$$

where δ_{ik} is the Kronecker delta. Using these relations and the property,

$$b_i|0\rangle = \langle 0|b_i^\dagger = 0 \tag{24}$$

enables equation (22) to be written

$$\langle ik|G|\ell m\rangle = (ik|g|\ell m) - (ik|g|m\ell) \tag{25}$$

If the initial and final states are the same, equation (25) yields

$$\langle ik|G|ik\rangle = (ik|g|ik) - (ik|g|ki) \tag{26}$$

Thus, the matrix elements of two-particle operators, in second quantization, are antisymmetric.

For an A-body state, the state vector is

$$|A\rangle = b_1^\dagger \ldots b_i^\dagger \ldots b_A^\dagger |0\rangle \tag{27}$$

Hence, for a two-body operator, equations (19) and (27) give

$$\langle A|G|A\rangle = \frac{1}{2} \sum_{ik} \sum_{\ell m} (ik|g|\ell m) \langle A|b_k^\dagger b_i^\dagger b_\ell b_m|A\rangle \tag{28}$$

which reduces to

$$\langle A|G|A\rangle = \frac{1}{2} \sum_{i,k=1}^{A} [(ik|g|ik) - (ik|g|ki)] \tag{29}$$

The Optical Potential

In second quantization notation, the state vector for the ground state of the projectile nucleus is

$$|P_0\rangle = p_1^\dagger \cdots p_j^\dagger \cdots p_{A_P}^\dagger |0\rangle \tag{30}$$

where $p_k^\dagger$ are projectile nucleon state creation operators. Similarly, the ground state of the target nucleus is

$$|T_0\rangle = g_1^\dagger \cdots g_\alpha^\dagger \cdots g_{A_T}^\dagger |0\rangle \tag{31}$$

where $g_\beta^\dagger$ are target nucleon state creation operators. Thus

$$W(\vec{x}) = \langle P_0 T_0 | V_{opt} | P_0 T_0 \rangle = \langle T_0 | \langle P_0 | V_{opt} | P_0 \rangle | T_0 \rangle \tag{32}$$

yields

$$W(\vec{x}) = \sum_{\beta k} \sum_{\alpha j} (\beta k | t | \alpha j) \langle T_0 | \langle P_0 | g_\beta^\dagger p_k^\dagger g_\alpha p_j | P_0 \rangle | T_0 \rangle \tag{33}$$

which reduces to

$$W(\vec{x}) = \sum_{\alpha=1}^{A_T} \sum_{j=1}^{A_P} [(\alpha j | t | \alpha j) - (\alpha j | t | j \alpha)] \tag{34}$$

The matrix elements are

$$(\alpha j | t | \alpha j) = \int d^3\vec{x}_\alpha \int d^3\vec{x}_j \; \phi_\alpha^\dagger(\vec{x}_\alpha) \; \phi_j^\dagger(\vec{x}_j) \; t_{\alpha j}(\vec{x}_\alpha, \vec{x}_j) \; \phi_\alpha(\vec{x}_\alpha) \; \phi_j(\vec{x}_j) \tag{35}$$

and

$$(\alpha j | t | j \alpha) = \int d^3\vec{x}_\alpha \int d^3\vec{x}_j \; \phi_\alpha^\dagger(\vec{x}_\alpha) \; \phi_j^\dagger(\vec{x}_j) \; t_{\alpha j}(\vec{x}_\alpha, \vec{x}_j) \; \phi_j(\vec{x}_\alpha) \; \phi_\alpha(\vec{x}_j) \tag{36}$$

In reference 7, the direct term in equation (34) was evaluated as

$$\sum_\alpha \sum_j (\alpha j | t | \alpha j) = A_P A_T \int d^3\vec{\xi}_T \; \rho_T(\vec{\xi}_T) \int d^3\vec{y} \; \rho_P(\vec{x}+\vec{y}+\vec{\xi}_T) \; \tilde{t}(e, \vec{y}) \tag{37}$$

which is equation (17). To evaluate the exchange term in equation (34), we rewrite equation (36) as

$$(\alpha j|t|j\alpha) = \int d^3\vec{x}_\alpha \int d^3\vec{x}_j \; \phi_\alpha^\dagger(\vec{x}_\alpha) \; \phi_j^\dagger(\vec{x}_j) \; t_{\alpha j}(\vec{x}_\alpha,\vec{x}_j) \; \phi_j(\vec{x}_\alpha) \; \phi_\alpha(\vec{x}_j) \left[\frac{\phi_\alpha(\vec{x}_\alpha) \; \phi_j(\vec{x}_j)}{\phi_\alpha(\vec{x}_\alpha) \; \phi_j(\vec{x}_j)}\right] \tag{38}$$

Rearranging the wave functions in equation (38) gives

$$(\alpha j|t|j\alpha) = \int d^3\vec{x}_\alpha \int d^3\vec{x}_j \; \phi_\alpha^\dagger(\vec{x}_\alpha) \; \phi_\alpha(\vec{x}_\alpha) \; \phi_j^\dagger(\vec{x}_j) \; \phi_j(\vec{x}_j) \; t_{\alpha j}(\vec{x}_\alpha,\vec{x}_j) \left[\frac{\phi_\alpha(\vec{x}_j) \; \phi_j(\vec{x}_\alpha)}{\phi_\alpha(\vec{x}_\alpha) \; \phi_j(\vec{x}_j)}\right] \tag{39}$$

Combining equations (34), (35), and (39) yields

$$W(\vec{x}) = \sum_{\alpha j} \int d^3\vec{x}_\alpha \int d^3\vec{x}_j \; \phi_\alpha^\dagger(\vec{x}_\alpha) \; \phi_\alpha(\vec{x}_\alpha) \; \phi_j^\dagger(\vec{x}_j) \; \phi_j(\vec{x}_j) \; t_{\alpha j}(\vec{x}_\alpha,\vec{x}_j)[1 - C_{\alpha j}(\vec{x}_\alpha,\vec{x}_j)] \tag{40}$$

with the correlation function given by

$$C_{\alpha j} = \frac{\phi_\alpha(\vec{x}_j) \; \phi_j(\vec{x}_\alpha)}{\phi_\alpha(\vec{x}_\alpha) \; \phi_j(\vec{x}_j)} \tag{41}$$

In terms of nuclear single-particle densities,

$$\rho(\vec{x}_i) = \phi_i^\dagger(\vec{x}_i) \; \phi_i(\vec{x}_i) \tag{42}$$

$W(\vec{x})$ becomes

$$W(\vec{x}) = \sum_{\alpha j} \int d^3\vec{x}_\alpha \; \rho_T(\vec{x}_\alpha) \int d^3\vec{x}_j \; \rho_P(\vec{x}_j) \; t_{\alpha j}(\vec{x}_\alpha,\vec{x}_j) \; [1 - C_{\alpha j}(\vec{x}_\alpha,\vec{x}_j)] \tag{43}$$

At this point, it is assumed that $C_{\alpha j}(\vec{x}_\alpha,\vec{x}_j)$ depends only upon the relative position of the α- and j-constituents. Then, the Fourier transform of equation (43) is

$$\tilde{W}(\vec{q}) = \sum_{\alpha j} t_{\alpha j}(e,\vec{q}) \; [1 - C_{\alpha j}(\vec{q})] \; F_T(\vec{q}) \; F_P(\vec{q}) \tag{44}$$

where the fact that $t_{\alpha j}$ depends only upon the relative position of the α- and j-constituents has been used. The form factors $F_T(\vec{q})$ and $F_P(\vec{q})$ are the Fourier transforms of the single-particle densities and $C_{\alpha j}(\vec{q})$ is the transform of the correlation function.

Following references 2, 3, and 7, the inverse Fourier transform of a single term in equation (44) is taken and then summed over all constituents to give

$$W(\vec{x}) = A_P A_T \int d^3\vec{\xi}_T \; \rho_T(\vec{\xi}_T) \int d^3\vec{y} \; \rho_P(\vec{x}+\vec{y}+\vec{\xi}_T) \; \tilde{t}(e,\vec{y}) \; [1 - \tilde{C}(\vec{y})] \tag{45}$$

where an approximation is made by introducing the average correlation function $\tilde{C}$ given by

$$\tilde{C} = \frac{1}{A_P A_T} \sum_{\alpha j} C_{\alpha j} \tag{46}$$

Equation (45) reduces to the previous result, equation (17), if there are no correlation effects (i.e., if $\tilde{C} \equiv 0$).

Correlation Function Approximation

Since $C_{\alpha j}$ in equation (41) depends explicitly on unknown nucleon single-particle wave functions $\phi_i(\vec{x}_i)$, the correlation function in equation (40) or (45) cannot be determined. Therefore, it must be approximated. One very good approximation, even for relatively light nuclei, is the infinite nuclear matter approximation (ref. 13) where the nucleon single-particle wave functions are assumed to be plane waves. The correlation function, from reference 13, is then written as

$$\tilde{C}(\vec{y}) = \frac{1}{4} \left[\frac{3 \; j_1(k_F y)}{k_F y} \right]^2 \tag{47}$$

where j_1 is the spherical Bessel function and $k_F = 1.36 \text{ fm}^{-1}$ is Fermi wave number. In this paper, for ease of analysis, the expression in equation (47) is replaced by a Gaussian form

$$C(\vec{y}) \approx \frac{1}{4} \exp(-0.18 y^2) \tag{48}$$

since

$$\left[\frac{3 \; j_1(k_F y)}{k_F y} \right]^2 = 1 - \frac{k_F^2 y^2}{10} + O(k_F^4 y^4) \tag{49}$$

and

$$\exp(-k_F^2 y^2) = 1 - \frac{k_F^2 y^2}{10} + O'(k_F^4 y^4) \tag{50}$$

agree for small values of $k_F y$ (i.e., when correlations are important).

RESULTS

Harmonic Well Density Distributions

Figures 1 through 6 display results for the charge and matter density distributions of lighter nuclei ($3 \leq Z \leq 8$) obtained from equations (1) and (14). Values for the charge distribution parameters a and α, taken from reference 5, are listed in table I for each of the nuclei. Analytic expressions for the nuclear matter density distributions in figures 1 through 6 can be parameterized as

$$\rho_m(r) = A_0(B_0 + C_0 r^2) \exp(-D_0 r^2) \tag{51}$$

where from equation (14),

$$\left.\begin{aligned} A_0 &= \frac{\rho_o a^3}{8s^3} \\ B_0 &= 1 + \frac{3\alpha}{2} - \frac{3\alpha a^2}{8s^2} \\ C_0 &= \frac{\alpha a^2}{16s^4} \\ D_0 &= \frac{1}{4s^2} \end{aligned}\right\} \tag{52}$$

Values for these matter density parameters are listed by nucleus in table II.

Heavy-Ion Total and Absorption Cross Sections

From eikonal scattering theory (ref. 14), the complex phase function is

$$\chi(\vec{b}) = -\frac{1}{2k} \int_{-\infty}^{\infty} U(\vec{b},z)\, dz \tag{53}$$

where $\vec{b}$ is projectile impact parameter, k is wave number, z is magnitude of the projectile position vector in the beam direction. The reduced potential U in terms of the optical potential $W(\vec{x})$ is

$$U(\vec{x}) = 2mA_P A_T (A_P + A_T)^{-1} W(\vec{x}) \tag{54}$$

Thus, the phase function, including Pauli correlation effects, is

$$\chi(\vec{b}) = \frac{1}{2} A_P A_T \sigma(e) [\alpha(e) + i] I(\vec{b}) \tag{55}$$

with

$$I(\vec{b}) = [2\pi B(e)]^{-3/2} \int d\vec{z} \int d^3\vec{\xi}_T \rho_T(\vec{\xi}_T) \int d^3\vec{y} \rho_P(\vec{b}+\vec{z}+\vec{y}+\vec{\xi}_T) [1 - \tilde{C}(\vec{y})] \exp \frac{-y^2}{2 B(e)} \tag{56}$$

Values for the nucleon-nucleon scattering parameters $\alpha(e)$, $\sigma(e)$, and $B(e)$ in equations (55) and (56) were taken from the compilations in references 15 and 16 and averaged over the projectile and target constituent types as in references 2, 3, 7, and 10. When computing cross sections, the correlation function approximation from equation (48) was incorporated into equation (56) for $\tilde{C}(\vec{y})$.

In terms of the complex phase function $\chi(\vec{b})$, the absorption cross section is

$$\sigma_{abs} = 2\pi \int_0^\infty \{1 - \exp[-2 \text{ Im } \chi(\vec{b})]\} b \, db \tag{57}$$

Table III displays representative absorption cross sections (from eqs. (55) to (57)) for carbon projectiles, at several different incident kinetic energies, colliding with various target nuclei. Also listed, for comparison, are theoretical predictions from reference 2 and available experimental data (refs. 17 through 20). The improved agreement between experimental results and the theoretical predictions in this work, over the predictions of reference 2, is primarily due to the use of the more precise harmonic well densities rather than the approximate Woods-Saxon distributions for lighter nuclei. Table IV shows that the effects on the absorption cross sections of including Pauli correlation were minimal. In general, the percentage reductions in cross sections were largest for lighter nuclear systems (low mass numbers) at lower incident kinetic energies. For a given collision pair (A_P, A_T), the percentage reduction decreases as the incident energy increases. For a given energy, the percentage reduction also decreases as system mass numbers increase. In all cases, however, the reductions in predicted absorption cross sections were less than 10 percent.

Table III reveals that the theoretical absorption cross sections from reference 2 are consistently smaller than those obtained in this work. This is a manifestation of the smaller surface thicknesses of the approximate Woods-Saxon densities,

used in reference 2, over the actual harmonic well surface thicknesses. The approximate Woods-Saxon densities used in reference 2 were obtained from more exact harmonic well distributions by artificially flattening the central charge densities (see ref. 4) at the expense of the longer range tail. The results of this artificial flattening for ^{12}C are displayed in figure 7. Note that the 90% to 10% region is smaller for the Woods-Saxon distribution than for the harmonic well distribution.

Figure 8 displays predicted absorption cross sections from this work and reference 2 for ^{16}O projectiles, at 2.1 GeV/nucleon, versus target mass number A_T. Also displayed are experimental results obtained by three experimental groups (refs. 18, 19, and 21). Again, the newer theoretical predictions are in better agreement with experiment than the predictions given in reference 2. As with the carbon projectile results of table III, the cross sections from reference 2 are smaller because of the artificial flattening of the oxygen charge density into a Woods-Saxon shape.

Collision total cross sections are obtained from

$$\sigma_{tot} = 4\pi \int_0^\infty \{1 - \exp[-\mathrm{Im}\ \chi(\vec{b})]\ \cos[\mathrm{Re}\ \chi(\vec{b})]\}\ b\ db \tag{58}$$

where the phase function, as before, is determined from equations (55) and (56). Table V gives results from equation (58) for ^{12}C-^{12}C collisions at two different laboratory kinetic energies. Also shown are theoretical predictions from reference 2 and experimental results from reference 17. The lack of agreement between the predictions of this work and the experimental results of reference 17 may be due to the large uncertainty in $\alpha(e)$ (around 60 percent at these energies) in Re $\chi(b)$. This uncertainty does not affect σ_{abs} because $\alpha(e)$ does not appear in equation (57). Varying $\alpha(e)$ between its limits of uncertainty (see ref. 2) varies σ_{tot} for ^{12}C-^{12}C collisions, at 2.1 GeV/nucleon, by 4 percent. This variation is sufficient to give agreement with the limited results of reference 17. Improvements to this phase of the theory would require either more accurate knowledge of $\alpha(e)$ or more experimental data for comparison, or both.

Projectile-Ion Abrasion Cross Sections

From reference 10, the cross section for abrading n projectile nucleons is

$$\sigma_n = \binom{A_P}{n} 2\pi \int \{1 - \exp[-A_T\ \sigma(e)\ I(\vec{b})]\}^n \exp[-A_T A_F\ \sigma(e)\ I(\vec{b})]\ b\ db \tag{59}$$

where the residual fragment (prefragment) mass number is

$$A_F = A_P - n \tag{60}$$

and $I(\vec{b})$ is given by equation (56). Results obtained from equation (59) are displayed in table VI for ^{20}Ne projectiles at 2.1 GeV/nucleon colliding with

^{12}C targets. Also displayed are abrasion results without Pauli correlations (i.e., $\tilde{C} = 0$ in eqs. (56) and (59)). For $n \leq 12$, correlation effects are insignificant. This results from the peripheral nature of these collisions where there is little overlap of the colliding nuclear volumes. As the number of abraded nucleons increases, greater volume overlap is required which results in larger correlation effects. The Pauli correlation contribution should be greatest when there is complete overlap of the colliding nuclear volumes. This situation occurs for $n = A_P = 20$ (i.e., $A_F = 0$) where, from table VI, the cross section is reduced by an order of magnitude from the uncorrelated result. Recall that V_{opt} in equation (16) is written in terms of free nucleon-nucleon transition amplitudes. In reality, the effective force in nuclear matter is much weaker than the free nucleon-nucleon force (ref. 22). This is manifested in the reduced cross sections obtained when exclusion principle correlation effects are included. For the results presented herein, the carbon target density parameters are those listed in tables I and II. For the ^{20}Ne projectile, the matter density is extracted, using the procedure in reference 2, from a Woods-Saxon charge distribution:

$$\rho_c(r) = \frac{\rho_o}{1 + \exp[(r - R)/c]} \tag{61}$$

with nuclear half-density radius R and nuclear surface thickness t given by (ref. 23)

$$R = 2.740 \text{ fm}$$

$$t = 2.515 \text{ fm}$$

and diffuseness c obtained from

$$c = t/4.4 \tag{62}$$

Until recently, no experimental abrasion data were available for comparison with theory. In the past, theoretical abrasion cross sections (which do not include important ablation effects) could only be compared with experimental fragmentation results (which do include ablation effects). Hence, experimental verification of a particular theoretical abrasion model was not possible. Recently, Stevenson et al. (refs. 24 and 25) have provided experimental abrasion measurements suitable for comparison with theory. Figures 9 and 10 display these experimental results for ^{20}Ne projectiles (at incident kinetic energy of 2.1 GeV/nucleon) colliding with a carbon target.

The experimental results are presented as relative probabilities for forming a particular projectile fragment residual mass A_F by abrading n nucleons from the incident projectile nucleus. These displayed results also include only those fragments with nuclear charge Z less than 10. This minimizes the likelihood of uninteracted beam particles being included in the data. The displayed mass distribution does not cut off sharply at $A_F = 20$ because of the finite resolution ($\approx$1.5 amu) of the detector (ref. 25). To compare theory with these experimental results, the theo-

retical abrasion cross sections must be converted into relative probabilities. Let the relative probability be

$$\text{R.P.} = \frac{\sigma_n}{\sigma'_{abs}} \tag{63}$$

where σ_n is obtained from equation (59) and

$$\sigma'_{abs} = \sigma_{abs} - 0.5\sigma_1 \tag{64}$$

In equation (64), σ_{abs} is given by

$$\sigma_{abs} = \sum_{n=1}^{A_P} \sigma_n \tag{65}$$

and the term, $0.5\sigma_1$, accounts for the ^{19}Ne fragments which are not included in the experimental data. Additionally, for $A_F = 19$, the relative probability is given by

$$\text{R.P.} = \frac{0.5\sigma_1}{\sigma'_{abs}} \tag{66}$$

since the ^{19}Ne fragments must be excluded.

As displayed in figure 9, the agreement between this theory and experiment is very good. Note also that the theory agrees better with the experiment when Pauli correlation effects are included. This is especially true for the lighter residual mass fragments. The slight disagreement between the theoretical predictions (with correlations) and experimental results may be indicative of the approximate nature of the infinite nuclear matter approximation to the actual correlation function. Unfortunately, improvements in this area are hindered by the lack of knowledge of the exact nuclear single-particle wave functions.

Finally, the marked improvement in the abrasion predictions of this work over those of the original version of this abrasion theory is displayed in figure 10. Recall that the original theory (ref. 10) used approximate Woods-Saxon densities for ^{12}C and did not include correlation effects. Surprisingly, both calculations yield comparable absorption cross sections (1057 mb for the theory in ref. 10 versus 1076 mb for this work).

CONCLUDING REMARKS

In this work, a previously developed heavy-ion reaction theory, capable of predicting total, absorption, and abrasion cross sections for heavy-ion collisions, has

been significantly improved in two ways. First, the accuracy of theoretical predictions for lighter nuclei (three to eight protons) was improved by developing an exact analytic expression for the correct harmonic well matter density distributions rather than approximating these by inexact artificially flattened Woods-Saxon distributions. Second, the need for Pauli exclusion principle correlation effects to be included in the theory has been identified and the theoretical framework extended to include them. Since exact analytical methods for calculating correlation functions require knowledge of the, as yet, unknown nuclear single-particle wave functions, an infinite matter approximation was satisfactorily implemented. These Pauli correlation effects were noted to be especially important for predicting those abrasion cross sections resulting from collisions involving large spatial overlap of the colliding nuclear volumes. Further theoretical improvements are presently being developed.

Langley Research Center
National Aeronautics and Space Administration
Hampton, VA 23665
March 5, 1982

REFERENCES

1. Satchler, G. R.; and Love, W. G.: Folding Model Potentials From Realistic Interactions for Heavy-Ion Scattering. Phys. Rep., vol. 55, no. 3, Oct. 1979, pp. 183-254.

2. Wilson, John W.; and Costner, Christopher M.: Nucleon and Heavy-Ion Total and Absorption Cross Section for Selected Nuclei. NASA TN D-8107, 1975.

3. Wilson, J. W.; and Townsend, L. W.: An Optical Model for Composite Nuclear Scattering. Canadian J. Phys., vol. 59, no. 11, Nov. 1981, pp. 1569-1576.

4. Hofstadter, R.; and Collard, H. R.: Nuclear Radii Determined by Electron Scattering. Landolt-Börnstein Numerical Data and Functional Relationships in Science and Technology, Group I, Vol. 2, H. Schopper, ed., Springer-Verlag, 1967, pp. 21-52.

5. De Jager, C. W.; De Vries, H.; and De Vries, C.: Nuclear Charge- and Magnetization-Density-Distribution Parameters From Elastic Electron Scattering. At. Data & Nucl. Data Tables, vol. 14, no. 5/6, Nov./Dec. 1974, pp. 479-508.

6. Bleszynski, M.; and Sander, C.: Geometrical Aspects of High-Energy Peripheral Nucleus-Nucleus Collisions. Nucl. Phys., vol. A326, nos. 2-3, Sept. 10, 1979, pp. 525-535.

7. Wilson, John W.: Composite Particle Reaction Theory. Ph. D. Diss., The College of William and Mary in Virginia, June 1975.

8. Überall, Herbert: Electron Scattering From Complex Nuclei, Part A. Academic Press, Inc., 1971, chapter 3.

9. Mayer, Maria Goeppert; and Jensen, J. Hans D.: Elementary Theory of Nuclear Shell Structure. John Wiley & Sons, Inc., 1955.

10. Townsend, Lawrence W.: Optical-Model Abrasion Cross Sections for High-Energy Heavy Ions. NASA TP-1893, 1981.

11. Borkowski, F.; Simon, G. G.; Walther, V. H.; and Wendling, R. D.: On the Determination of the Proton RMS-Radius From Electron Scattering Data. Z. Phys. A, vol. 275, no. 1, 1975, pp. 29-31.

12. Eder, Gernot (Irving Kaplan, transl.): Nuclear Forces - Introduction to Theoretical Nuclear Physics. The M.I.T. Press, c.1968, chapter 13.

13. Bohr, Aage; and Mottelson, Ben R.: Nuclear Structure. Volume I - Single-Particle Motion. W. A. Benjamin, Inc., 1969, chapter 2.

14. Joachain, Charles J.: Quantum Collision Theory. American Elsevier Pub. Co., Inc., 1975, chapter 9.

15. Hellwege, K.-H., ed.: Elastische und Ladungsaustausch-Streuung von Elementarteilchen. Landolt-Bornstein Numerical Data and Functional Relationships in Science and Technology, Group I, Vol. 7, Springer-Verlag, 1973.

16. Benary, Odette; Price, Leroy R.; and Alexander, Gideon: NN and ND Interactions (Above 0.5 GeV/c) - A Compilation. UCRL-20000 NN, Lawrence Radiation Lab., Univ. of California, Aug. 1970.

17. Jaros, J.; Wagner, A.; Anderson, L.; Chamberlain, O.; Fuzesy, R. Z.; Gallup, J.; Gorn, W.; Schroeder, L.; Shannon, S.; Shapiro, G.; and Steiner, H.: Nucleus-Nucleus Total Cross Sections for Light Nuclei at 1.55 and 2.89 GeV/c per Nucleon. Phys. Rev., ser. C, vol. 18, no. 5, Nov. 1978, pp. 2273-2292.

18. Heckman, H. H.; Greiner, D. E.; Lindstrom, P. J.; and Shwe, H.: Fragmentation of ^{4}He, ^{12}C, ^{14}N, and ^{16}O Nuclei in Nuclear Emulsion at 2.1 GeV/Nucleon. Phys. Rev., ser. C, vol. 17, no. 5, May 1978, pp. 1735-1747.

19. Cheshire, D. L.; Huggett, R. W.; Johnson, D. P.; Jones, W. V.; Rountree, S. P.; Verma, S. D.; Schmidt, W. K. H.; Kurz, R. J.; Bowen, T.; and Krider, E. P.: Fragmentation Cross Sections of 2.1-GeV/Nucleon ^{12}C and ^{16}O Ions. Phys. Rev., ser. D, vol. 10, no. 1, July 1974, pp. 25-31.

20. Skrzypczak, E.: Cross-Sections for Inelastic ^{4}He and ^{12}C-Nucleus Collisions at 4.5 GeV/c/N Incident Momentum. Proceedings of the International Conference on Nuclear Physics, Volume 1, Abstracts, LBL-11118 (Contract No. W-7405-ENG-48), Lawrence Berkeley Lab., Univ. of California, Aug. 1980, p. 575.

21. Jakobsson, B.; and Kullberg, R.: Interactions of 2 GeV/Nucleon ^{16}O With Light and Heavy Emulsion Nuclei. Phys. Scr., vol. 13, no. 6, June 1976, pp. 327-338.

22. Preston, M. A.; and Bhaduri, R. K.: Structure of the Nucleus. Addison-Wesley Pub. Co., Inc., 1975, chapter 8.

23. Knight, E. A.; Singhal, R. P.; Arthur, R. G.; and Macauley, M. W. S.: Elastic Scattering of Electrons From $^{20,22}Ne$. J. Phys. G.: Nucl. Phys., vol. 7, no. 8, Aug. 1981, pp. 1115-1121.

24. Stevenson, J.; Martinis, J.; and Price, P. B.: Measurement of the Total Energy of Projectile Fragments in Relativistic Heavy-Ion Collisions. Bull. American Phys. Soc., vol. 26, no. 4, Apr. 1981, p. 540.

25. Stevenson, J. D.; Martinis, J.; and Price, P. B.: Measurement of the Summed Residual Projectile Mass in Relativistic Heavy-Ion Collisions. Phys. Rev. Lett., vol. 47, no. 14, Oct. 5, 1981, pp. 990-993.

SYMBOLS

A	nuclear mass number
A_0	defined in equations (52), fm^{-3}
a	oscillator parameter, fm
$B(e)$	average slope parameter of nucleon-nucleon scattering amplitude, fm^2
B_0	defined in equations (52)
$\vec{b}$	projectile impact parameter vector, fm
b_ℓ	annihilation operator for ℓth single-particle state
$b_\ell^\dagger$	creation operator for ℓth single-particle state
$C_{\alpha j}$	correlation function between α- and j-constituents
$\tilde{C}$	average correlation function
C_0	defined in equations (52), fm^{-2}
c	speed of light, m/sec
D_0	defined in equations (52), fm^{-2}
e	two-nucleon kinetic energy in their center of mass frame, GeV
$F(q)$	nuclear form factor
G	unspecified two-body operator in equation (19)
$g_\alpha, g_\alpha^\dagger$	annihilation and creation operators for target α-constituent state
$I(\vec{b})$	defined in equation (56)
Im $\chi(\vec{b})$	imaginary part of eikonal phase shift function
n	number of abraded nucleons
$p_j, p_j^\dagger$	annihilation and creation operators for projectile j-consituent state
$\vec{q}$	momentum transfer vector, fm^{-1}
Re $\chi(\vec{b})$	real part of eikonal phase shift function, dimensionless
$\vec{r}$	position vector, fm

r_p	proton root-mean-square charge radius, fm
s	defined in equation (12)
$\tilde{t}$	average two-nucleon transition amplitude, MeV
$t_{\alpha j}$	two-nucleon transition operator for nucleons α and j, MeV
V_{opt}	optical potential operator, MeV
$W(\vec{x})$	optical potential (defined in eqs. (17) and (45)), MeV
$\vec{x}$	relative position vector of projectile ($\vec{x} = \vec{b} + \vec{z}$), fm
$\vec{y}$	two-nucleon relative position vector, fm
Z	total number of nuclear protons
$\vec{z}$	position vector of projectile in beam direction, fm
$\binom{A}{n}$	binomial coefficient
α	harmonic well distribution parameter (see eq. (2))
$\alpha(e)$	average ratio of real part to imaginary part of nucleon-nucleon scattering amplitude
$\vec{\xi}_T$	collection of constituent relative coordinates for target, fm
ρ	nuclear density, fm^{-3}
ρ_o	normalization constant in equation (1), fm^{-3}
$\sigma(e)$	average nucleon-nucleon total cross section, fm^2 or mb
σ_{abs}	heavy-ion absorption cross section, fm^2 or mb
σ_{exp}	experimental heavy-ion cross section, fm^2 or mb
σ_n	cross section for abrading n nucleons, fm^2 or mb
σ_{tot}	heavy-ion total cross section, fm^2 or mb
ϕ	nuclear single-particle wave function $(fm)^{-3/2}$
$\chi(\vec{b})$	eikonal phase shift function
ψ	nuclear two-body wave function $(fm)^{-3}$

Subscripts:

c	charge
F	prefragment
m	matter
P	projectile
p	proton
T	target

Arrows over symbols indicate vectors.

TABLE I.- NUCLEAR CHARGE DISTRIBUTION PARAMETERS

FROM ELECTRON SCATTERING DATA

[From ref. 5]

Nucleus	α	a, fm
^{7}Li	0.327	1.77
^{9}Be	.611	1.791
^{11}B	.811	1.69
^{12}C	1.247	1.649
^{14}N	1.291	1.729
^{16}O	1.544	1.833

TABLE II.- HARMONIC WELL MATTER DENSITY DISTRIBUTION PARAMETERS

Nucleus	A_0, fm^{-3}	B_0	C_0, fm^{-2}	D_0, fm^{-2}
^{7}Li	0.0282	0.906	0.148	0.380
^{9}Be	.0211	.829	.268	.370
^{11}B	.0225	.739	.419	.425
^{12}C	.0190	.571	.691	.452
^{14}N	.0156	.607	.625	.402
^{16}O	.0112	.591	.636	.350

TABLE III.- ABSORPTION CROSS SECTIONS FOR ^{12}C PROJECTILES COLLIDING WITH VARIOUS TARGET NUCLEI

A_T	σ_{abs}, mb		σ_{exp}, mb
	This work	Ref. 2	
0.87 GeV/nucleon			
12	819	763	[a]939 ± 49
2.1 GeV/nucleon			
1	237	246	[a]269 ± 14 [b]258 ± 21
12	839	781	[a]888 ± 50 [b]826 ± 23
16	990	820	[b]1022 ± 25
64	1727	1656	[b]1730 ± 36
138	2519	2447	[c]2600 ± 100
184	2924		[c]3000 ± 100
208	3047	2969	[b]2960 ± 65
3.6 GeV/nucleon			
12	836	779	[d]780 ± 30
20	1059	902	[d]1040 ± 60
64	1723	1653	[d]1700 ± 90

[a]Reference 17.
[b]Reference 18.
[c]Reference 19.
[d]Reference 20.

TABLE IV.- PAULI CORRELATION EFFECTS ON ABSORPTION CROSS SECTIONS FOR SELECTED COLLISION PAIRS

Collision pair	Incident kinetic energy, GeV/nucleon	σ_{abs}, mb		Reduction in σ_{abs}, percent
		Without correlation	With correlation	
Ne + C	3.6	1144	1059	7.4
O + Cu	.1	2059	1951	5.2
	2.1	2055	1952	5.0
	22.5	2039	1940	4.8
O + Pb	.1	3416	3341	2.2
	2.1	3418	3346	2.1
	22.5	3403	3333	2.0

TABLE V.- TOTAL CROSS SECTIONS FOR ^{12}C-^{12}C SCATTERING

Incident kinetic energy, GeV/nucleon	σ_{tot}, mb		σ_{exp}, mb (ref. 17)
	This work	Ref. 2	
0.87	1348	1293	1256 ± 54
2.1	1413	1348	1347 ± 53

TABLE VI.- OPTICAL MODEL ABRASION CROSS SECTIONS FOR THE REACTION $^{20}Ne + {}^{12}C \rightarrow n + X$

[Incident kinetic energy is 2.1 GeV/nucleon]

Number of abraded nucleons, n	Abrasion cross sections, mb	
	With Pauli correlation	Without Pauli correlation
1	248	248
2	134	134
3	95	95
4	76	75
5	64	64
6	57	56
7	52	51
8	48	48
9	45	45
10	43	43
11	42	42
12	40	42
13	38	42
14	33	41
15	27	39
16	18	33
17	10	25
18	4	14
19	1	6
20	0.1	1

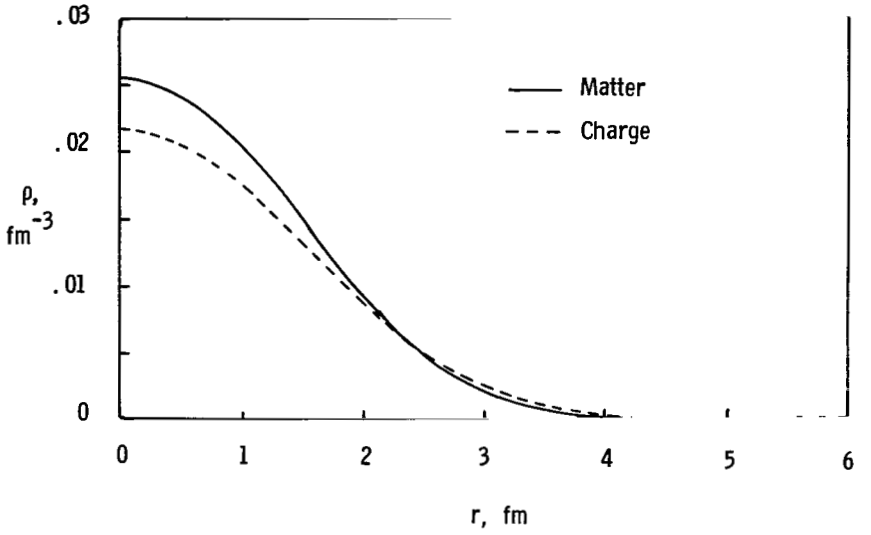

Figure 1.- Harmonic well charge and matter density distributions for ^{7}Li.

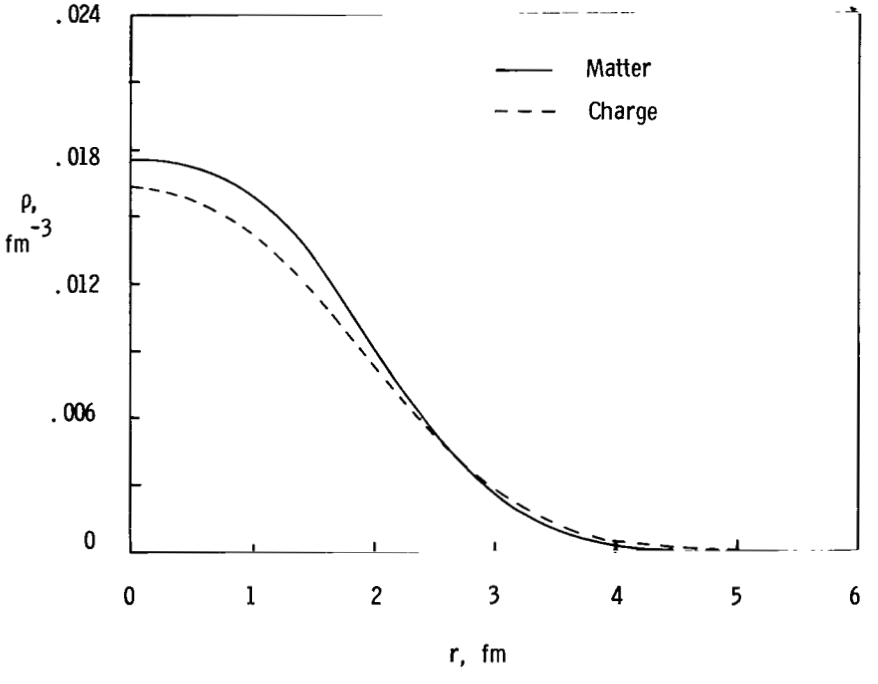

Figure 2.- Harmonic well charge and matter density distributions for ^{9}Be.

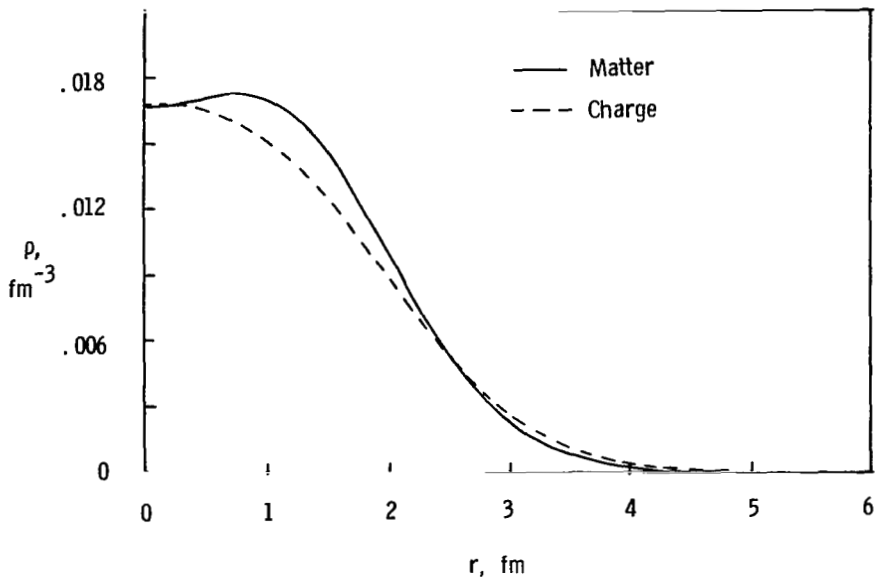

Figure 3.- Harmonic well charge and matter density distributions for ^{11}B.

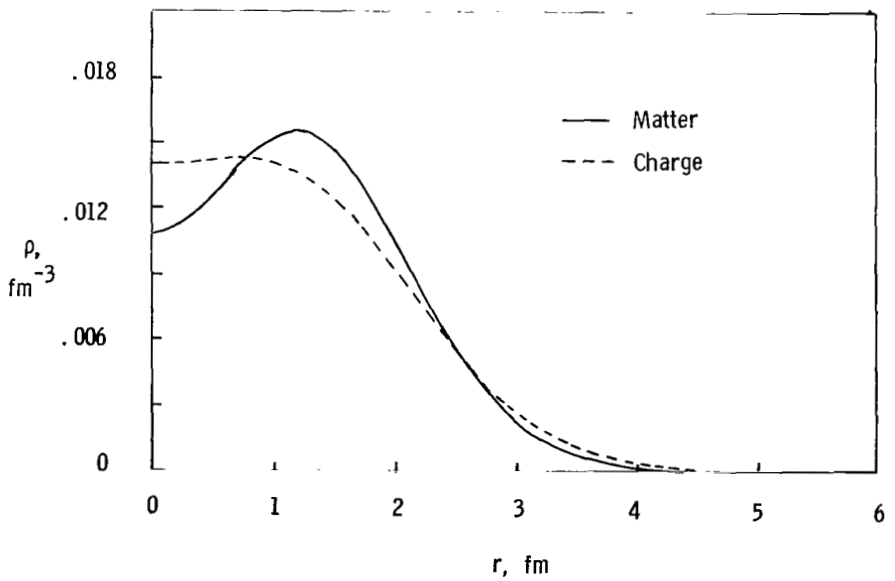

Figure 4.- Harmonic well charge and matter density distributions for ^{12}C.

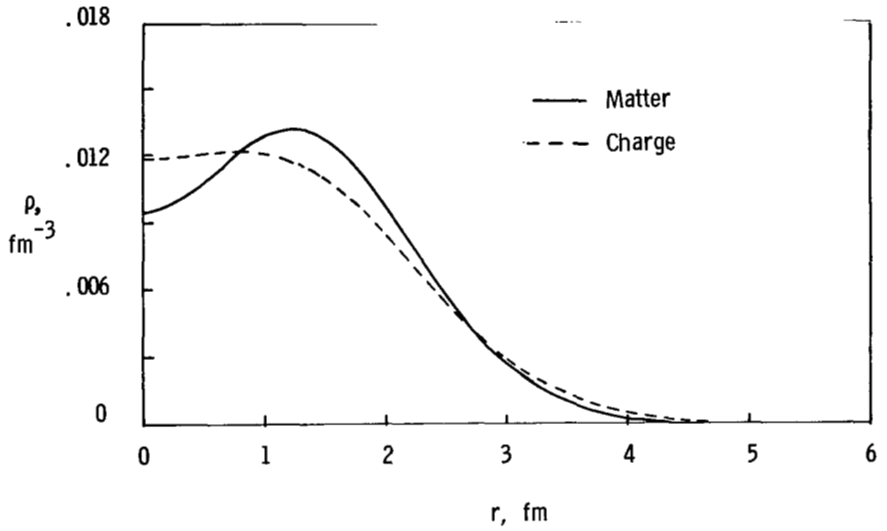

Figure 5.- Harmonic well charge and matter density distributions for ^{14}N.

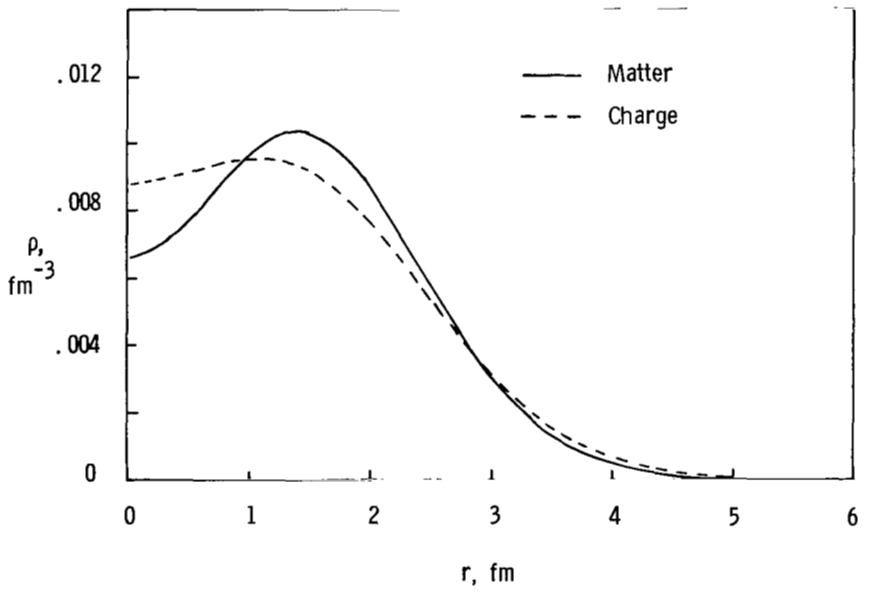

Figure 6.- Harmonic well charge and matter density distributions for ^{16}O.

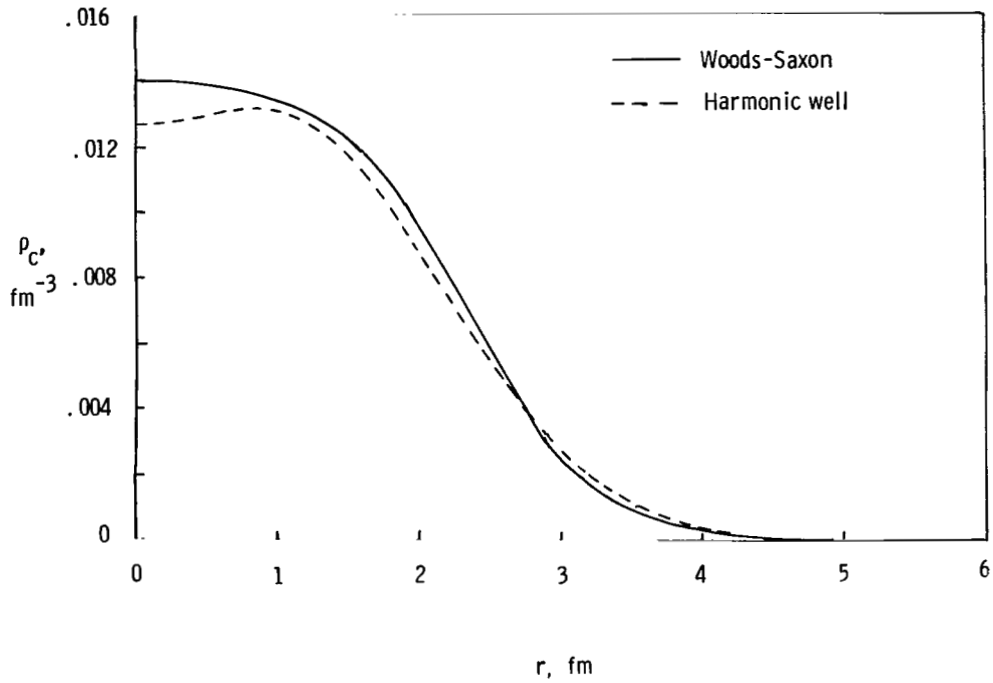

Figure 7.- ^{12}C harmonic well charge distribution and the Woods-Saxon density obtained by artificially flattening it.

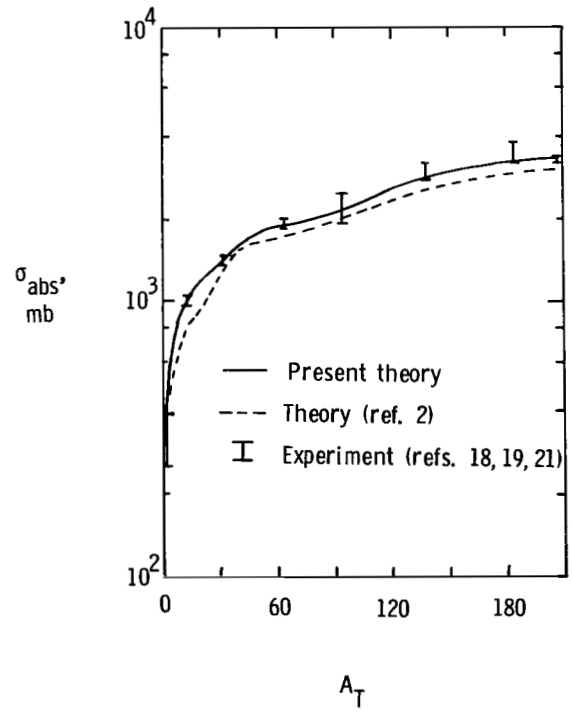

Figure 8.- Absorption cross sections for ^{16}O projectiles. Incident kinetic energy is 2.1 GeV/nucleon.

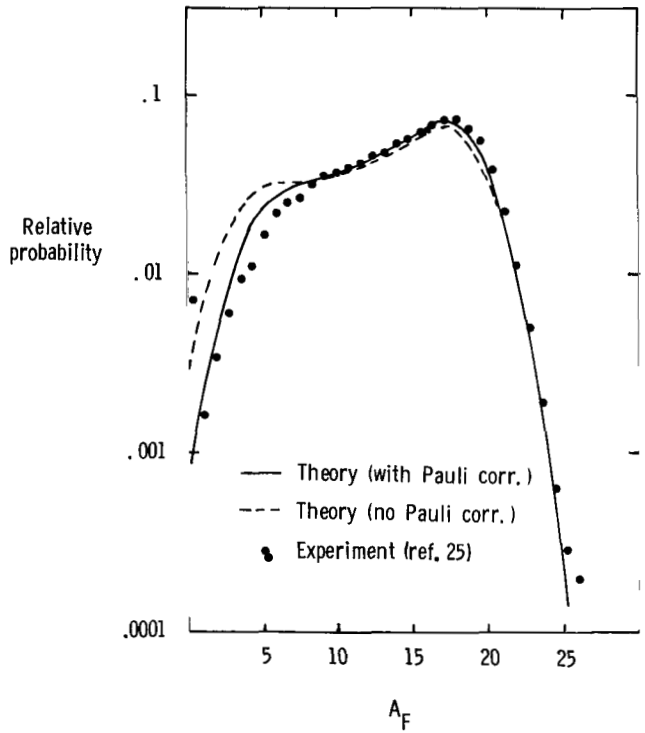

Figure 9.- Theoretical abrasion results (with and without the Pauli correlation correction) compared with experiment for ^{20}Ne projectiles colliding with ^{12}C targets. Incident kinetic energy is 2.1 GeV/nucleon.

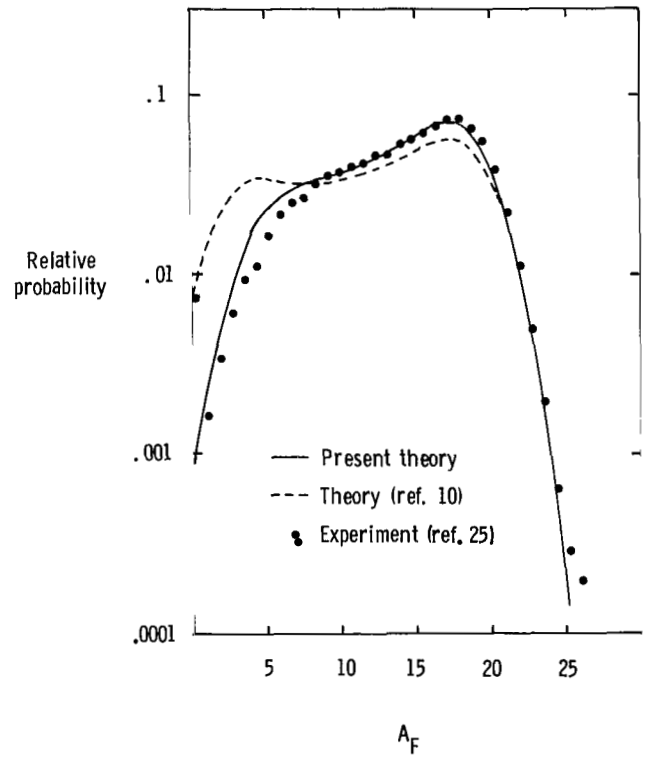

Figure 10.- Abrasion results for ^{20}Ne projectiles colliding with ^{12}C targets predicted in this work compared with a previous theoretical model (ref. 10) and with experiment. Incident kinetic energy is 2.1 GeV/nucleon.

1. Report No.	2. Government Accession No.	3. Recipient's Catalog No.
NASA TP-2003		

4. Title and Subtitle	5. Report Date
HARMONIC WELL MATTER DENSITIES AND PAULI CORRELATION EFFECTS IN HEAVY-ION COLLISIONS	April 1982
	6. Performing Organization Code 199-20-76-01
7. Author(s)	8. Performing Organization Report No. L-15105
Lawrence W. Townsend	10. Work Unit No.
9. Performing Organization Name and Address	11. Contract or Grant No.
NASA Langley Research Center Hampton, VA 23665	13. Type of Report and Period Covered Technical Paper
12. Sponsoring Agency Name and Address	14. Sponsoring Agency Code
National Aeronautics and Space Administration Washington, DC 20546	

15. Supplementary Notes

16. Abstract

A generalized optical-model heavy-ion reaction theory is extended to include correlation effects between projectile and target constituents according to the Pauli exclusion principle. These correlation effects are found to be significant for accurately predicting cross sections for projectile-nucleus abrasion, but are relatively unimportant for determining total and absorption cross sections for heavy-ion collisions. For lighter nuclei, predictive capabilities were also improved by developing an analytic method for extracting their nuclear single-particle density distributions from experimentally measured harmonic well charge density distributions. This improved theory is compared with previous theoretical predictions and recent experimental results.

17. Key Words (Suggested by Author(s))	18. Distribution Statement
Heavy ions Projectile fragmentation Exclusion principle correlations Nuclear matter densities	Unclassified - Unlimited Subject Category 73

19. Security Classif. (of this report)	20. Security Classif. (of this page)	21. No. of Pages	22. Price
Unclassified	Unclassified	29	A03

For sale by the National Technical Information Service, Springfield, Virginia 22161

NASA-Langley, 1982